The Numerov Process Over A Non-Uniform Grid

Rossella Brunetti
University of Modena and Reggio Emilia: Universita degli Studi di Modena e Reggio Emilia
Nicolò Attilio Speciale
Universita di Bologna
Massimo Rudan (Massimo.Rudan@unibo.it)
University of Bologna https://orcid.org/0000-0001-5485-7067

Research Article

Keywords: Numerov process, Non-uniform grid, Semiconductor-device model, Box-integration method

Posted Date: February 24th, 2021

DOI: https://doi.org/10.21203/rs.3.rs-229482/v1

Version of Record: A version of this preprint was published at Journal of Computational Electronics on April 13th, 2021. See the published version at https://doi.org/10.1007/s10825-021-01699-3.

Journal of Computational Electronics manuscript No.
(will be inserted by the editor)

The Numerov process over a non-uniform grid

R. Brunetti · N. Speciale · M. Rudan

Received: date / Accepted: date

Abstract The Numerov process is a solution method applicable to some classes of differential equations, that provides an error term of the fifth order in the grid size with a computational cost comparable to that of the finite-difference scheme. In the original formulation of the method, a uniform grid size is required; the paper shows a procedure for extending its applicability to a non-uniform grid in one dimension. The effectiveness of the procedure is tested on a model problem. Next, a variable transformation is described, that reduces the mathematical model of semiconductor devices to a form tractable with the Numerov process. Such a transformation is considered also in the multi-dimensional case, where it is shown that it solves a long-lasting difficulty in semiconductor modeling, namely, the impossibility of reconstructing the current density over the grid elements.

Keywords Numerov process · Non-uniform grid · Semiconductor-device model · Box-integration method

1 Introduction

The *Numerov Process* (NP [8], cited in [2]) is applicable to the solution of some classes of differential equations; its error term is $O(h^5)$, with h the grid size, much superior to that of the finite-difference scheme, with a comparable computational cost. In the original formulation of NP, a uniform grid is necessary,

R. Brunetti
FIM Department, University of Modena and Reggio Emilia, Via Campi 213/A, I-41125 Modena, Italy
Tel.: +39-059-205-8371
E-mail: rossella.brunetti@unimore.it

N. Speciale and M. Rudan
"E. De Castro" Advanced Research Center on Electronic Systems (ARCES) and Department DEI, University of Bologna, Viale del Risorgimento 2, I-40136 Bologna, Italy.

which is a drawback for many practical applications; more recently, a method for extending the scheme to a variable step in one dimension has been shown [16]. This paper shows an approach, different from that of [16], for extending NP to a non-uniform grid in one dimension; the approach preserves the accuracy of the original NP by combining the latter with a numerical integration having the same order of error.

The interest in highly-accurate schemes derives, among others, from the need of solving the transport model of semiconductor devices, which is fundamental for the integrated-circuit technology. Unfortunately, the form of the semiconductor-device model as it stands is such, that NP is not applicable. In the paper, a variable transformation is shown that makes the semiconductor model tractable with the one-dimensional, variable-step version of NP.

The last part of the paper deals with the effect of the variable transformation on the multi-dimensional form of the semiconductor model. It is shown that, when the standard Box-Integration Method is used on the transformed equations, all physical quantities of interest are well defined over the discretization elements, even if a general grid, different from a tensor-product one, is used. This solves a long-lasting difficulty in semiconductor modeling: in fact, when the standard solution methods are used, the current density turns out to be ill defined over the discretization elements; this, in turn, produces errors in the calculation of the current at contacts, and in the analysis of physical effects driven by the current density. The variable transformation eliminates the problem.

The paper is organized as follows: the extension of NP to a one-dimensional, non-uniform grid is shown in Sect. 2, and the properties of the matrix derived from it are outlined in Sect. 3; the application to a model problem, along with the comparison with the finite-difference scheme, is shown in Sect. 4 using different grids. A comparison with the approach of [16] is carried out in Sect. 5. The variable transformation that reduces the semiconductor model to a form suitable for the application of NP is shown in Sect. 6, and the calculation of the equations coefficients is carried out in Sect. 7. The effect of using the transformed equations in more than one dimension is discussed in Sect. 8 and, finally, the conclusions are drawn in Sect. 9.

2 The Numerov Process over a Non-uniform Grid

We start by considering the one-dimensional, second-order equation of the form

$$-u'' = F(u, x)\,, \tag{1}$$

where the dependence of F on u may be non linear. The standard Numerov Process (NP) requires a uniform grid (the derivation of NP is shown in the Appendix); uniformity is necessary because NP is based on series expansions, and the uniform spacing of the grid points makes the odd powers of the right

and left expansions to cancel each other. After eliminating the odd powers, one determines the even powers in terms of u by recursively applying (1); this is also the reason why it is necessary to consider a form like (1) of the equation, where the first derivative of the unknown function does not appear.

To extend NP to a non-uniform grid one must preserve the possibility to cancel, albeit only locally, the odd powers of the expansions. An approach that fulfills this requirement is shown here, which combines a formally exact solution over a non-uniform grid with the improved precision of NP. Consider a one-dimensional, non-uniform grid with N internal nodes, namely, $x_0 < x_1 < \cdots < x_N < x_{N+1}$, and let $h_{i+1} = x_{i+1} - x_i$ be the size of one of its elements. With reference to (1), for any $x_{i-1} \le x \le x_i$ it is

$$u'(x) = u'_{i-1} - \int_{x_{i-1}}^{x} F(u,\xi)\,\mathrm{d}\xi\,. \tag{2}$$

Repeating on the next element $x_i \le x \le x_{i+1}$, and integrating again, yields

$$u(x) = u_i + u'_i\,(x - x_i) - \int_{x_i}^{x} (x-\xi)\,F(u,\xi)\,\mathrm{d}\xi\,. \tag{3}$$

Fixing the second integration limit transforms (2), (3) into

$$u'_i = u'_{i-1} - \int_{x_{i-1}}^{x_i} F(u,x)\,\mathrm{d}x\,, \qquad i = 1, 2, \ldots \tag{4}$$

$$u_{i+1} = u_i + h_{i+1}\,u'_i - \int_{x_i}^{x_{i+1}} (x_{i+1}-x)\,F(u,x)\,\mathrm{d}x\,, \qquad i = 0, 1, \ldots \tag{5}$$

The problem is thus shifted to the calculation of the two integrals

$$G_i = \int_{x_{i-1}}^{x_i} F(u,x)\,\mathrm{d}x\,, \qquad H_{i+1} = \int_{x_i}^{x_{i+1}} (x_{i+1}-x)\,F(u,x)\,\mathrm{d}x\,. \tag{6}$$

Due to the form of F, integrals (6) depend on u, but not on u'. If G_i and H_{i+1} are approximated with formulas where only the nodal values of u appear, namely, $G_i = G_i(u_{i-1}, u_i)$ and $H_{i+1} = H_{i+1}(u_i, u_{i+1})$, the resulting expressions do not introduce extra unknowns with respect to those that explicitly appear in (4) and (5). As shown later, this goal can be accomplished in a manner that exploits the precision of NP.

Assuming that integrals (6) have been calculated, the way in which the nodal values of u are found from (4), (5) depends on the boundary conditions. If the boundary conditions u_0, u'_0 are given, the starting point is calculating u_1 from (5) after letting $i = 0$ there; to calculate u_2 one needs u'_1, which is obtained by letting $i = 1$ in (4); then, one proceeds recursively until the Nth node is reached.

If, instead, the boundary conditions u_0, u_{N+1} are given (which is the typical case in, e.g., the numerical analysis of semiconductor devices), one must eliminate the first derivatives from the system (4), (5). For this, one rearranges (4)

to find $G_i = u'_{i-1} - u'_i$, then solves (5) for u'_i to find $u'_i = (u_{i+1} - u_i + H_{i+1})/h_{i+1}$; shifting the index in the latter expression then yields $u'_{i-1} = (u_i - u_{i-1} + H_i)/h_i$ which, combined with the former, provides

$$\frac{u_i - u_{i-1}}{h_i} - \frac{u_{i+1} - u_i}{h_{i+1}} = G_i - \frac{H_i}{h_i} + \frac{H_{i+1}}{h_{i+1}}\,; \tag{7}$$

then, one manipulates the term $G_i - H_i/h_i$ in order to give (7) the more symmetric form

$$\frac{u_i - u_{i-1}}{h_i} - \frac{u_{i+1} - u_i}{h_{i+1}} =$$

$$= \int_{x_{i-1}}^{x_i} \frac{x - x_{i-1}}{h_i} F(u,x)\,\mathrm{d}x + \int_{x_i}^{x_{i+1}} \frac{x_{i+1} - x}{h_{i+1}}\,F(u,x)\,\mathrm{d}x\,. \tag{8}$$

So far, no approximation has been introduced; to calculate the integrals in (8) one now applies Simpson's rule

$$\int_a^b \omega\,\mathrm{d}x \simeq (b-a)\,\frac{\omega(a) + 4\,\omega(c) + \omega(b)}{6}\,, \tag{9}$$

with c the midpoint of $[a,b]$. The error term of (9) is $\mathrm{O}[(b-a)^5\,\omega^{(4)}]$, with $\omega^{(4)}$ the 4th derivative of ω calculated at some point of the integration interval [9].

Using index $i-1/2$ to denote the quantities at the midpoint of h_i, index $i+1/2$ to denote those at the midpoint of h_{i+1}, and applying (9), transforms (8) into

$$-\frac{u_{i-1}}{h_i} + \left(\frac{1}{h_i} + \frac{1}{h_{i+1}}\right) u_i - \frac{u_{i+1}}{h_{i+1}} =$$

$$= \frac{1}{3}\,\left(h_i\,F_{i-1/2} + \frac{h_i + h_{i+1}}{2}\,F_i + h_{i+1}\,F_{i+1/2}\right)\,. \tag{10}$$

One notes that the left hand side of (10) corresponds to the discretization of the second derivative obtained from a parabolic interpolation over a non-uniform grid; in turn, the central term of the right hand side (without the 1/3 factor) is the discretized form of the right hand side of $-u'' = F$ when the finite-difference method is used (compare with (22)). The improvement inherent in (10) derives from Simpson's rule whose error term, as mentioned above, is $\mathrm{O}(h_i^5)$ in the interval on the left of x_i and $\mathrm{O}(h_{i+1}^5)$ in the interval on the right of it. The issue is to calculate the values $F_{i-1/2}$ and $F_{i+1/2}$, that belong to the midpoint of each interval.

3 The System Matrix

From the discussion carried out at the end of the Appendix one may assume that the equation in hand has been linearized and that the solution is being carried out by iterations; therefore, within the single iteration the dependence of F on u is linear, say, $F = c(x)\,u + s(x)$, whence $F_{i-1/2} = c_{i-1/2}\,u_{i-1/2} + s_{i-1/2}$ and $F_{i+1/2} = c_{i+1/2}\,u_{i+1/2} + s_{i+1/2}$; Eq. (10) then becomes

$$-\frac{u_{i-1}}{h_i} + \left(\frac{1}{h_i} + \frac{1}{h_{i+1}} - \frac{h_i + h_{i+1}}{6}\,c_i\right)\,u_i - \frac{u_{i+1}}{h_{i+1}} =$$

$$= \frac{1}{3}\,\left(h_i\,c_{i-1/2}\,u_{i-1/2} + h_{i+1}\,c_{i+1/2}\,u_{i+1/2}\right) +$$

$$+\frac{1}{3}\,\left(h_i\,s_{i-1/2} + \frac{h_i + h_{i+1}}{2}\,s_i + h_{i+1}\,s_{i+1/2}\right)\,. \tag{11}$$

Considering the case of the semiconductor-device model, the result expressed by (11) is applicable also to the Poisson equation (shown in (26) below); in fact, letting $u \leftarrow w$, $s \leftarrow \zeta$, $c \leftarrow 0$ provides

$$-\frac{w_{i-1}}{h_i} + \left(\frac{1}{h_i} + \frac{1}{h_{i+1}}\right)\,w_i - \frac{w_{i+1}}{h_{i+1}} =$$

$$= \frac{1}{3}\,\left(h_i\,\zeta_{i-1/2} + \frac{h_i + h_{i+1}}{2}\,\zeta_i + h_{i+1}\,\zeta_{i+1/2}\right)\,. \tag{12}$$

Coming back to (11), the values of c and s at the nodes and at the midpoints of the elements are known, because the two functions are either prescribed or, like in the case considered here, are taken from the previous step of an iterative procedure. In contrast, $u_{i-1/2}$ and $u_{i+1/2}$ are not known; however, u is the solution of (1), for which the NP interpolation (52) holds because the three nodes considered are equally spaced. For $u_{i-1/2}$, replicating (52) over the three nodes in hand yields

$$-\left(1 + \frac{h_i^2}{48}\,c_{i-1}\right)\,u_{i-1} + \left(2 - 10\,\frac{h_i^2}{48}\,c_{i-1/2}\right)\,u_{i-1/2} - \left(1 + \frac{h_i^2}{48}\,c_i\right)\,u_i =$$

$$= \frac{h_i^2}{48}\,\left(s_{i-1} + 10\,s_{i-1/2} + s_i\right)\,, \tag{13}$$

namely, $u_{i-1/2} = a_i^{i-1}\,u_{i-1} + a_i^i\,u_i + h_i^2\,b_i^{i-1/2}$ with

$$a_i^{i-1} = \frac{48 + h_i^2\,c_{i-1}}{96 - 10\,h_i^2\,c_{i-1/2}}\,, \qquad a_i^i = \frac{48 + h_i^2\,c_i}{96 - 10\,h_i^2\,c_{i-1/2}}\,,$$

$$b_i^{i-1/2} = \frac{s_{i-1} + 10\,s_{i-1/2} + s_i}{96 - 10\,h_i^2\,c_{i-1/2}}\,. \tag{14}$$

Similarly, $u_{i+1/2} = a^i_{i+1}\, u_i + a^{i+1}_{i+1}\, u_{i+1} + h^2_{i+1}\, b^{i+1/2}_{i+1}$ with

$$a^i_{i+1} = \frac{48 + h^2_{i+1}\, c_i}{96 - 10\, h^2_{i+1}\, c_{i+1/2}}\,, \qquad a^{i+1}_{i+1} = \frac{48 + h^2_{i+1}\, c_{i+1}}{96 - 10\, h^2_{i+1}\, c_{i+1/2}}\,,$$

$$b^{i+1/2}_{i+1} = \frac{s_i + 10\, s_{i+1/2} + s_{i+1}}{96 - 10\, h^2_{i+1}\, c_{i+1/2}}\,. \tag{15}$$

Replacing the expressions of $u_{i-1/2}$ and $u_{i+1/2}$ into (11) and rearranging, yields

$$-\beta_i\, u_{i-1} + \alpha_i\, u_i - \gamma_i\, u_{i+1} = \sigma_i + \eta_i\,, \tag{16}$$

with

$$\beta_i = \frac{1}{h_i} + \frac{a^{i-1}_i\, h_i}{3}\, c_{i-1/2}\,, \qquad \gamma_i = \frac{1}{h_{i+1}} + \frac{a^{i+1}_{i+1}\, h_{i+1}}{3}\, c_{i+1/2}\,, \tag{17}$$

$$\alpha_i = \frac{1}{h_i} + \frac{1}{h_{i+1}} - \frac{a^i_i\, h_i}{3}\, c_{i-1/2} - \frac{h_i + h_{i+1}}{6}\, c_i - \frac{a^i_{i+1}\, h_{i+1}}{3}\, c_{i+1/2}\,, \tag{18}$$

$$\sigma_i = \frac{h_i}{3}\, s_{i-1/2} + \frac{h_i + h_{i+1}}{6}\, s_i + \frac{h_{i+1}}{3}\, s_{i+1/2}\,,$$

$$\eta_i = \frac{b^{i-1/2}_i h^3_i}{3}\, c_{i-1/2} + \frac{b^{i+1/2}_{i+1} h^3_{i+1}}{3}\, c_{i+1/2}\,. \tag{19}$$

In conclusion, by combining the Simpson rule with an interpolation of the NP type, integrals (8) have been calculated in terms of the nodal values u_{i-1}, u_i, u_{i+1} only, and the accuracy of NP has been kept. No constraint has been imposed on the elements; as a consequence, the scheme is applicable to a general, non uniform grid. The outcome of the whole procedure is the $N \times N$ algebraic system (16).

One notes that the system matrix of (16) is tridiagonal like in the finite-difference scheme; however, it is not symmetric because $\gamma_{i-1} \neq \beta_i$ due to the fact that $a^{i-1}_i \neq a^i_i$; the asymmetry is not to be ascribed to the non uniformity of the grid, nor to the use of NP, but to the presence of term $c\, u$ in the equation to be solved. In fact, even if a uniform grid is used, the matrix resulting from it is still asymmetric (compare with (52)); conversely, if it happens that $c = \text{const}$, then (14) renders $a^{i-1}_i = a^i_i$ and makes the matrix symmetric.

4 Model Problem

In this section we consider a model problem useful for an experimental validation of the procedure outlined in Sects. 2 and 3; we take the interval $0 \le x \le 1$ and assume that the solution of $-u'' = c\,u + s$ is

$$u = \lambda\,\sin(\lambda)\,, \qquad \lambda(x) = k\,\pi\,\frac{1+p}{1+p\,x}\,, \tag{20}$$

with k, p two positive integers, so that the boundary conditions are $u(0) = u(1) = 0$. One finds

$$c = (\omega\,\lambda)^2\,(\lambda^2 - 2)\,, \qquad s = -4\,(\omega\,\lambda)^2\,\lambda^2\,\cos(\lambda)\,, \qquad \omega = \frac{p}{k\,\pi\,(1+p)}\,. \tag{21}$$

Function (20) is such that the frequency and amplitude of the oscillations increase from right to left; the case corresponding to $k = 2$ and $p = 5$ is considered (function (20) is shown as the green line in Figs. 1 and 2). Equation $-u'' = c\,u + s$, with coefficients given by (21), is solved on different grids using the generalized NP method of Sects. 2 and 3, or the standard finite-difference scheme (FD); the latter yields

$$-\frac{u_{i-1}}{h_i} + \left(\frac{1}{h_i} + \frac{1}{h_{i+1}}\right)\,u_i - \frac{u_{i+1}}{h_{i+1}} = \frac{h_i + h_{i+1}}{2}\,\left(c_i\,u_i + s_i\right)\,. \tag{22}$$

Each outcome is compared with the true solution (20); more specifically, as error indicators we adopt

$$\epsilon_{\rm FD} = \max_i |u_i^{\rm FD} - u_i|\,, \qquad \epsilon_{\rm NP} = \max_i |u_i^{\rm NP} - u_i|\,, \tag{23}$$

where $u_i^{\rm FD}$ or $u_i^{\rm NP}$ is the value of the solution obtained at the ith node using the FD or NP scheme, and u_i is the value of (20) at the same node.

The first comparison has been carried out by randomly generating the nodal positions within the integration domain; other comparisons have been carried out starting from a uniform grid, whose nodes have subsequently been shifted to obtain a prescribed density of nodes over the integration domain. Specifically, the shift was obtained by defining the new nodal positions y_i, $i = 1, \ldots, N$ with the transformation

$$y = \frac{1 + p - \sqrt{1 + p\,(p+2)\,(1-x)}}{p}\,, \qquad 0 \le y \le 1\,, \tag{24}$$

where p is the positive integer appearing in the definition (20). Observing that the nodal density of the uniform grid is $Q = 1/(N+1)$, and that the density $g(y)$ of the shifted grid fulfills the relation $Q\,{\rm d}x = g(y)\,{\rm d}y$, one finds

$$g(y) = \frac{2}{N+1}\,\frac{1 + p\,(1-y)}{p+2}\,. \tag{25}$$

Table 1 Error indicators (23) obtained using randomly-generated grids.

N	ϵ_{FD}	ϵ_{NP}
10,000	0.8	6×10^{-5}
5,000	1.5	4×10^{-4}
2,500	33	7×10^{-2}
2,000	40	8×10^{-2}
1,000	—	0.4
600	—	3.2
550	—	28

Table 2 Error indicators (23) obtained using uniform grids.

N	ϵ_{FD}	ϵ_{NP}
5,000	0.4	3.7×10^{-6}
2,000	2.7	1.4×10^{-4}
1,000	12	2.3×10^{-3}
500	65	3.6×10^{-2}
250	—	0.6
150	—	3.7
100	—	13

In particular it is $g(0) = (p+1)\, g(1)$, namely, the ratio $g(0)/g(1)$ is the same as $\lambda(0)/\lambda(1)$, where λ is the parameter appearing in the definition (20) of u. With respect to the original positions pertaining to the uniform grid, transformation (24) shifts the nodes to the left, namely, in the direction where the frequency and amplitude of u increase.

The error indicators (23) are shown in the tables for different numbers of grid nodes N; specifically, Tab. 1 shows the results obtained from the randomly-generated grids, Tab. 2 those of uniform grids, and Tab. 3 those of the left-shifted grids (although considering uniform grids is redundant with respect to the scope of this work, the results are shown for comparison with those of the other cases). In each set of simulations, the number of nodes has progressively been reduced until the error indicator (23) reached a value of the same order as the oscillation amplitude of u; it is interesting to note that the increase in the error exhibits a sort of threshold: this is visible, for instance, in the right column of Tab. 1 when the number of nodes is decreased from 600 to 550, and also in the other tables, both in the FD column and in the NP one.

Considering the general trend of the error indicator, the tables show that, as expected, the error improves from the case of the randomly-generated grids, to that of the uniform grids and, finally, to that of the left-shifted grids. As for the comparison between the two solution methods, it is found in all cases that the non-uniform NP is better by orders of magnitude than the corresponding FD.

Table 3 Error indicators (23) obtained using left-shifted grids.

N	ϵ_{FD}	ϵ_{NP}
5,000	0.2	5×10^{-7}
2,000	1	2×10^{-5}
1,000	4	3×10^{-4}
750	7	9×10^{-4}
500	18	4×10^{-3}
250	—	7×10^{-2}
150	—	5×10^{-1}
75	—	7

5 Comparison with other approaches

An extension of NP to a non-uniform, one-dimensional grid has been proposed by Vigo-Aguiar and Ramos as a special case of the variable k-step Cowell method [16]. One of the outcomes of [16] (indicated here as VR from the authors' initials) is determining a strategy for selecting the length of element h_{i+1}, given $h_1, \ldots, h_i$, when solving (1) when the initial conditions $u(x_0) = u_0$, $u'(x_0) = u'_0$ are prescribed; as shown by examples provided in [16], VR is applicable also to boundary-value problems. In the following, the comparison is carried out using again the model problem $-u'' = c\,u + s$ with coefficients given by (20, 21); the method proposed here is compared with VR and with the boundary-value problem solver of MATLAB® [7] (the latter will be indicated with ML below).

Remembering the description of the present method given in Sects. 2, 3, the equation to be solved is recast in integral form and the integral over each element is calculated by the Simpson rule; for the latter, the value of u at the element's midpoint is needed, which is obtained from the NP interpolation (52). It may be argued that the introduction of such a "ghost" point in the middle of each element is equivalent to doubling the number of nodes, which is of advantage when the error indicator (23) is used. For this reason, another set of simulations have been carried out with VR using a double number of nodes with respect to that used with NP; the results of such simulations (which are more expensive in terms of computing time, see Tab. 5) are labeled VR2.

Table 4 compares the error indicators of type (23) obtained with different solution methods. The table has been obtained by solving (1) using ML with six different values of its internal relative-tolerance parameter. This provided six non-uniform grids, whose numbers of nodes are given in column N; the corresponding error indicators are shown in column ϵ_{ML}. Then, using the same grids, the solutions and the corresponding error indicators have been calculated again using the VR method with N nodes (ϵ_{VR}), the VR method with $2\,N$ nodes (ϵ_{VR2}), and the non-uniform-grid NP method (ϵ_{NP}). The solutions corresponding to the last two lines of Tab. 4 are shown in Figs. 1 and 2, respectively, for ML and NP, that exhibit the smallest error indicators.

Table 4 Error indicators (23) obtained with different solution methods (see text).

N	ϵ_{ML}	ϵ_{VR}	ϵ_{VR2}	ϵ_{NP}
986	6.6×10^{-5}	5.9×10^{-1}	1.7×10^{-1}	2.0×10^{-5}
527	1.0×10^{-3}	8.0×10^{-1}	1.0×10^{0}	3.2×10^{-4}
285	1.2×10^{-2}	2.8×10^{0}	4.1×10^{0}	4.1×10^{-3}
153	1.3×10^{-1}	3.0×10^{0}	5.1×10^{0}	5.4×10^{-2}
86	1.2×10^{0}	2.2×10^{2}	6.0×10^{1}	2.1×10^{-1}
76	5.1×10^{0}	3.3×10^{2}	2.9×10^{2}	1.7×10^{0}

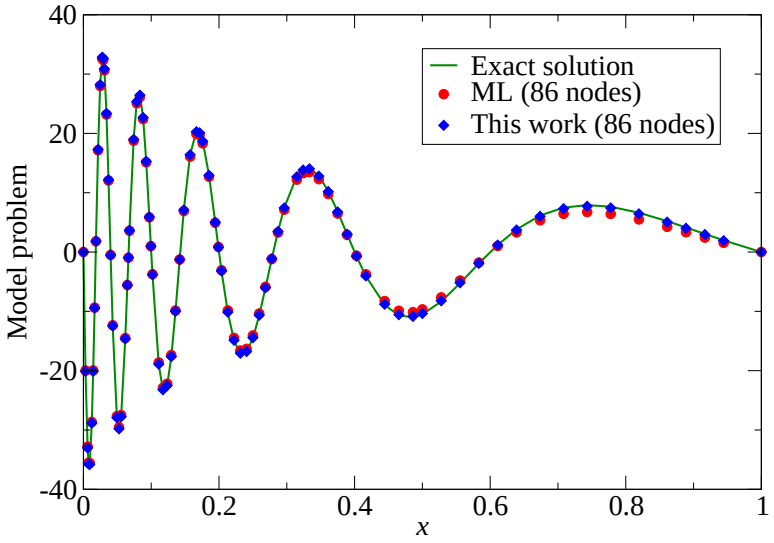

Fig. 1 Comparison between the solution of the model problem obtained over an 86-node grid using ML (red circles) and the method of this work (blue diamonds). The green line shows the exact solution of the same problem (the values of the parameters in (20) are $k = 2$, $p = 5$).

A last set of runs have been carried out to compare ϵ_{FD}, ϵ_{VR}, and ϵ_{NP} over randomly-generated grids (Fig. 3), and over initially-uniform grids shifted by applying the (24) scheme (Fig. 4). Finally, Tab. 5 compares the simulation time obtained with the different methods over a uniform grid; each time is normalized with respect to that of the non-uniform NP method.

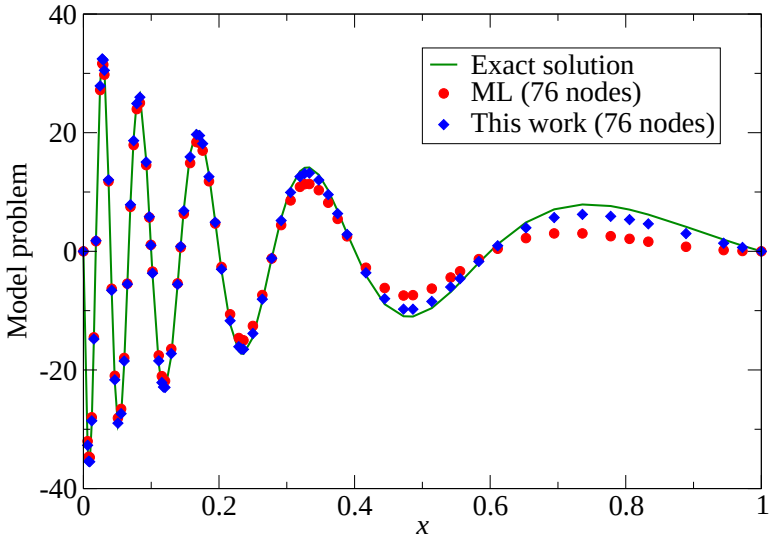

Fig. 2 Comparison between the solution of the model problem obtained over a 76-node grid using ML (red circles) and the method of this work (blue diamonds). The green line shows the exact solution of the same problem (the values of the parameters in (20) are $k = 2$, $p = 5$).

Table 5 Simulation time over a uniform grid, normalized with respect to that of the non-uniform NP method.

N	FD	VR	VR2
5,000	1.0×10^{0}	8.3×10^{-1}	1.3×10^{1}
2,500	2.6×10^{1}	1.3×10^{1}	9.5×10^{1}
2,000	1.1×10^{1}	1.3×10^{1}	6.6×10^{1}
1,000	9.7×10^{0}	6.2×10^{0}	4.1×10^{1}
750	5.6×10^{-1}	4.3×10^{-1}	2.7×10^{0}
500	5.7×10^{0}	4.2×10^{0}	2.6×10^{1}
250	2.6×10^{0}	2.4×10^{0}	1.0×10^{1}
150	2.7×10^{0}	2.1×10^{0}	1.3×10^{1}
100	1.3×10^{2}	4.7×10^{0}	1.4×10^{1}
75	3.4×10^{2}	3.9×10^{0}	4.5×10^{1}

6 Auxiliary Unknown for the Semiconductor-Device Model

An interesting application of NP over a non-uniform grid refers to the mathematical model of semiconductor devices. In the typical situations encountered in this field, the unknown functions of the model (electric potential and carrier concentrations) exhibit sharp variations in some regions of the semiconductor

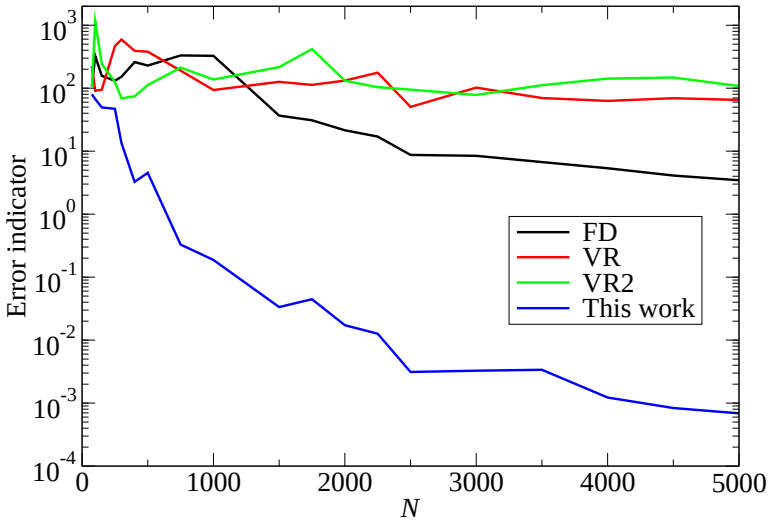

Fig. 3 Error indicators (23) obtained by solving the model problem (20) over randomly-generated grids using the FD (black line), the VR (red line), the VR2 (green line), and the non-uniform NP method (blue line). The horizontal axis shows the number of grid nodes.

domain, and vary little in others. For this reason, the extension of NP to the non-uniform grid is of interest. This section and Sect. 7 show how the semiconductor model can be reduced to a form amenable to the application of NP, namely, a form where the first derivatives of the unknowns do not appear. Results of application of the solution scheme to specific devices will be shown elsewhere; preliminary results over uniform grids have been presented in [14], [15].

6.1 The Semiconductor-Device Model

The mathematical model of semiconductor devices is made of the Poisson equation and of one or more moments of the Boltzmann Transport Equation (BTE) for the electrons and for the positively-charged carriers (holes). The model equations are coupled because the right hand side of the Poisson equation depends on the electron and hole concentrations, and the moments of the BTE depend on the electric field. The Poisson equation reads

$$-\varepsilon \nabla^2 \varphi = \varrho \,, \qquad -\nabla^2 w = \zeta \,, \tag{26}$$

with φ the electric potential, ϱ the charge density, and ε the permittivity; the corresponding normalized quantities are $w = q\,\varphi/(k_B\,T)$ and $\zeta = q\,\varrho/(\varepsilon\,k_B\,T)$,

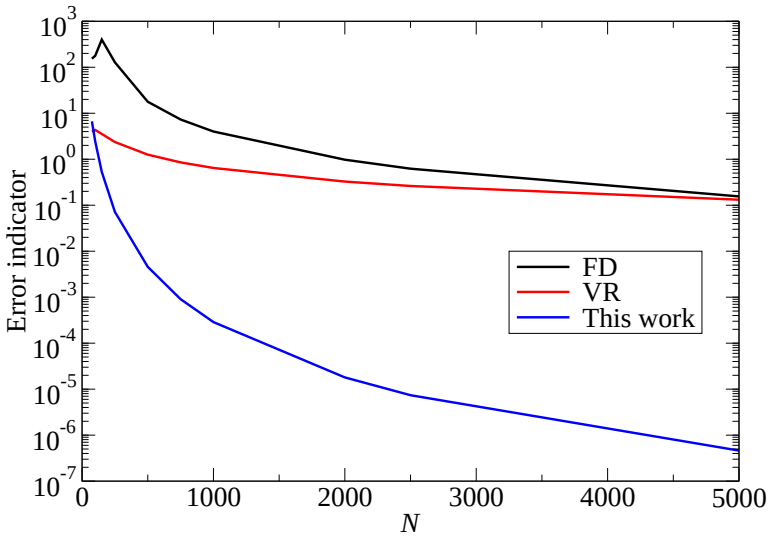

Fig. 4 Error indicators (23) obtained by solving the model problem (20) over initially-uniform grids shifted by applying the (24) scheme, using the FD (black line), the VR (red line), and the non-uniform NP method (blue line). The horizontal axis shows the number of grid nodes.

with q the electron charge, k_B the Boltzmann constant, and T the semiconductor temperature. The charge density depends on the concentrations n and p of electrons and holes, and on the electric potential. As the latter dependence is non linear, it is necessary to linearize the second of (26) around some tentative solution $\bar{w}$ and proceed by iterations; this yields an equation in the new unknown δw (compare with (54)):

$$-\nabla^2 \delta w = \chi\, \delta w + \tau\,, \qquad \chi = \left(\frac{\partial \zeta}{\partial w}\right)_{\bar{w}}\,, \qquad \tau = \nabla^2 \bar{w} + \zeta(\bar{w}, n, p)\,. \tag{27}$$

The moments of the BTE must be considered in pairs (details are found in [10]): the single pair $(0, 1)$, made of the moments of order zero and one, yields the *drift-diffusion* model; the two pairs $(0, 1)$ and $(2, 3)$ yield the *hydrodynamic model*, and so on. As each pair has the same structure, to the purpose of illustrating the procedure it suffices to consider the lowest pair $(0, 1)$. This is done here with reference to the electrons of the conduction band of the semiconductor, in the steady-state condition. The drift-diffusion model for the electrons reads

$$\operatorname{div} \boldsymbol{J}_n = q\, U\,, \qquad \boldsymbol{J}_n = -q\, \mu_n\, n\, \operatorname{grad} \varphi + q\, D_n\, \operatorname{grad} n\,, \tag{28}$$

with n, $\boldsymbol{J}_n$ the electron concentration and current density, respectively, U the net recombination rate, and μ_n, $D_n = \mu_n\, k_B\, T/q$ the electron mobility and diffusivity, respectively. For simplicity μ_n, and consequently D_n, are taken constant.

6.2 The Auxiliary Unknown

Letting $\boldsymbol{S} = \boldsymbol{J}_n/(q\, D_n)$ one recasts (28) in the normalized form $\operatorname{div} \boldsymbol{S} = U/D_n$, $\boldsymbol{S} = \operatorname{grad} n - n \operatorname{grad} w$; then, introducing the auxiliary unknown $u = n \exp(-w/2)$ transforms (28) into

$$-\nabla^2 u = c\, u + s\,, \qquad c = \frac{\zeta}{2} - \frac{|\operatorname{grad} w|^2}{4}\,, \qquad s = -\frac{U}{D_n} \exp(-w/2)\,. \quad (29)$$

Note that the transformation leading to (29) is not a reduction to the self-adjoint form, which would in fact read $\operatorname{div}\{\exp(w) \operatorname{grad}[n \exp(-w)]\} = U/D_n$, nor an exponential fitting like the one typically adopted for solving the semiconductor equations, which would read $[n \exp(-w)]' = S \exp(-w)$ with $S =$ const over the segment connecting two nodes (the exponential-fitting scheme is also known as *Scharfetter-Gummel method* [13]; more on this in Sect. 9). The first derivatives of the unknown are missing from (27) and (29), whose one-dimensional form is, respectively,

$$-\delta w'' = \chi\, \delta w + \tau\,, \qquad -u'' = c\, u + s\,; \quad (30)$$

in conclusion, the semiconductor-device model has been recast in a form that makes NP applicable. The final step, shown in Sect. 7, is calculating the coefficients of each equation with a precision consistent with that of NP.

7 Calculation of the coefficients

The coefficients of (27) depend on the values of $\bar{w}$ and of the carrier concentration(s) at each node and at the elements' midpoints. The nodal values are taken from the previous iteration, those at midpoints are calculated from the former through expressions of the form (13). As far as (29) is concerned, the one-dimensional form of the coefficients reads

$$c = \frac{\zeta}{2} - \frac{|w'|^2}{4}\,, \qquad s = -\frac{U}{D_n} \exp(-w/2)\,, \quad (31)$$

which entails the calculation of the derivative w' at the nodes and at the element midpoints. For the midpoint values one adapts (50) to the case in hand, to find

$$w'_{i-1/2} = \frac{w_i - w_{i-1}}{h_i} + \frac{h_i}{24}\,(\zeta_i - \zeta_{i-1})\,,$$
$$w'_{i+1/2} = \frac{w_{i+1} - w_i}{h_{i+1}} + \frac{h_{i+1}}{24}\,(\zeta_{i+1} - \zeta_i)\,. \quad (32)$$

For the nodal points, instead, one adapts (5), to find

$$w_{i+1} = w_i + h_{i+1}\, w'_i - \int_{x_i}^{x_{i+1}} (x_{i+1} - x)\, \zeta(x)\, \mathrm{d}x\,. \tag{33}$$

Using the same procedure as above for calculating the integral, one finds

$$\begin{aligned} w'_i &= \frac{w_{i+1} - w_i}{h_{i+1}} + \int_{x_i}^{x_{i+1}} \frac{x_{i+1} - x}{h_{i+1}}\, \zeta(x)\, \mathrm{d}x = \\ &= \frac{w_{i+1} - w_i}{h_{i+1}} + \frac{h_{i+1}}{6}\, \left(\zeta_i + 2\, \zeta_{i+1/2}\right)\,. \end{aligned} \tag{34}$$

The asymmetry of (34) is cured by repeating the procedure to the left of x_i; this yields

$$w_{i-1} = w_i - h_i\, w'_i - \int_{x_{i-1}}^{x_i} (x - x_{i-1})\, \zeta(x)\, \mathrm{d}x\,, \tag{35}$$

$$\begin{aligned} w'_i &= \frac{w_i - w_{i-1}}{h_i} - \int_{x_{i-1}}^{x_i} \frac{x - x_{i-1}}{h_i}\, \zeta(x)\, \mathrm{d}x = \\ &= \frac{w_i - w_{i-1}}{h_i} - \frac{h_i}{6}\, \left(2\, \zeta_{i-1/2} + \zeta_i\right) \end{aligned} \tag{36}$$

whence, taking the half sum of (34) and (36),

$$\begin{aligned} w'_i &= \frac{w_i - w_{i-1}}{2\, h_i} + \frac{w_{i+1} - w_i}{2\, h_{i+1}} + \\ &+ \frac{1}{6}\, \left(h_{i+1}\, \zeta_{i+1/2} - h_i\, \zeta_{i-1/2} + \frac{h_{i+1} - h_i}{2}\, \zeta_i\right)\,. \end{aligned} \tag{37}$$

8 The auxiliary unknown in more than one dimension

The natural evolution of this research line is the extension of the method to more than one dimension. The extension of NP to the multi-dimensional case using tensor-product grids has been achieved for uniformly-spaced grids (in [6], with reference to the Schrödinger equation, and in [14], [15], with reference to the semiconductor-device model), whereas that to non-uniform, tensor-product grids has not been achieved yet.

In semiconductor-device analysis, due to the complex form of the integration domain and to the presence of internal interfaces between different materials, an even more general type of grid is often adopted, whose elements are simplexes: considering for instance a two-dimensional case, the grid is made of triangular elements like those shown in Fig. 5. The triangles correspond to the elements like h_i or h_{i+1} of the one-dimensional case; the domain with the red boundary is the Wigner-Seitz cell of node P_i, and its sides are the axes of the triangles' sides emanating from P_i; such a domain corresponds to the $(h_i + h_{i+1})/2$ cell of the one-dimensional case. In constructing the grid, care is

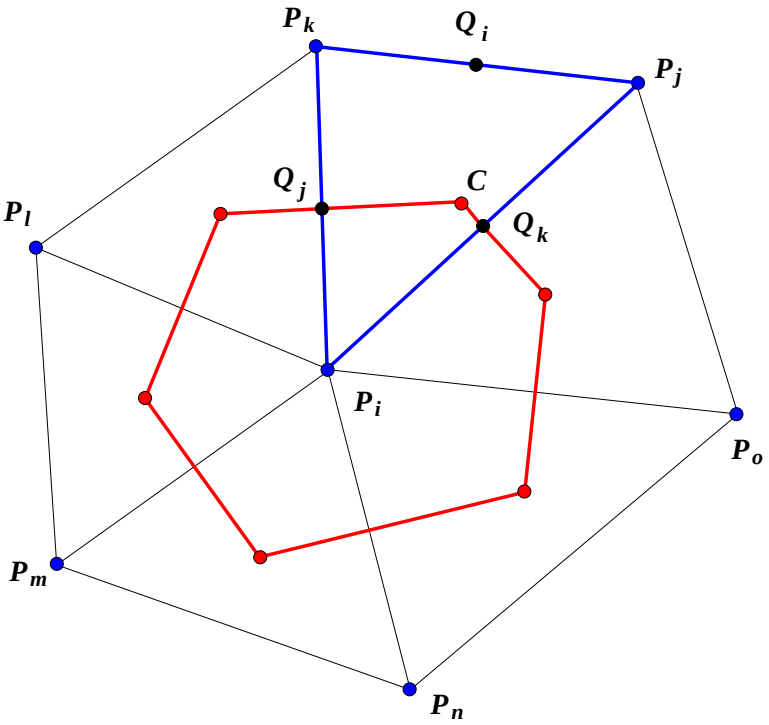

Fig. 5 Example of triangle-based grid used in the simulation of semiconductor devices in two dimensions.

taken to avoid obtuse triangles; in this way, the circumcenter C of a triangle always belongs to the interior or the boundary of it.

The typical method for solving the Poisson equation (27) on this grid consists in applying the Gauss theorem over the Wigner-Seitz cell, and in approximating the area integral at the right hand side by replacing the integrand with a constant:

$$-\int_{\partial\Omega_i} \mathrm{grad}(\delta w)\cdot\boldsymbol{\nu}\,\partial\Omega = \int_{\Omega_i} (\chi\,\delta w+\tau)\,\mathrm{d}\Omega \simeq \Omega_i\,(\chi_i\,\delta w_i+\tau_i)\,, \qquad (38)$$

with Ω_i the area of the cell, $\partial\Omega_i$ its boundary, and $\boldsymbol{\nu}$ the outward unit vector normal to $\partial\Omega_i$. In turn, the flux at the left hand side of (38) is approximated by replacing δw with a linear function over each triangle; in this way the contribution of, e.g., the blue triangle to the flux is $\overline{CQ}_k\,(\delta w_i-\delta w_j)/\overline{P_iP}_j + \overline{CQ}_j\,(\delta w_i-\delta w_k)/\overline{P_iP}_k$. This procedure, also called *Box-Integration Method*

(BIM), has become popular for solving the drift-diffusion model since the late 70s [3], [1], and has subsequently been extended to the higher moments of the BTE [11], [12], [4], [5].

When BIM is applied to the transport part of the model, the vector equation like, e.g., the second of (28) or its normalized form $\boldsymbol{S} = \operatorname{grad} n - n \operatorname{grad} w$, is projected onto the sides of each triangle, and the projection is approximated with a constant over the side itself; the resulting expression $[n \exp(-w)]' = S \exp(-w)$, with $S = \text{const}$, is integrated over each side, this providing the exponential-fitting scheme mentioned in Sect. 6; finally, the result is used in the calculation of the flux across the cell boundary $\partial\Omega_i$.

A drawback of the exponential-fitting scheme is that the current density is not well defined over each triangle: one finds a different vector depending on which pair of projections one uses to reconstruct the current from the scalar components. This is due to the fact that, apart from the special case of a purely-diffusive transport, the current density is not a gradient; therefore, forcing its components to be constant along arbitrarily-oriented directions introduces an inconsistency. In the practical applications, the impossibility of reconstructing the current-density vector introduces an error in the calculation of the currents at the device contacts, and in the analysis of physical effects driven by current density like, e.g., impact ionization.

The variable transformation leading to the form (29) of the transport model eliminates the drawback: the equation to be solved is in fact identical to the linearized Poisson equation (27); therefore, it can be solved with BIM with respect to u (given w), using the same approximations. The dependence of the electron concentration on the coordinates is extracted from $n = u \exp(w/2)$ only after the solution is achieved; also, combining $\boldsymbol{S} = \operatorname{grad} n - n \operatorname{grad} w$ with $n = u \exp(w/2)$ yields, for each triangle, the normalized current density in terms of u and w:

$$\boldsymbol{S} = \exp(w/2) \left(\operatorname{grad} u - u \operatorname{grad} w/2\right). \tag{39}$$

The above equation defines uniquely $\boldsymbol{S}$, which turns out to be quite different from a constant. This result shows that the variable transformation $u = n \exp(-w/2)$, which in one dimension makes it possible to implement NP thanks to the elimination of the first derivative, is also beneficial when the multi-dimensional version of the transport model in semiconductors is considered: thanks again to the elimination of the first derivatives, all physical quantities of interest are in fact well defined over the grid elements.

9 Conclusions

A method for extending the Numerov process to a non-uniform grid in one dimension has been shown. The result is achieved by acting on each grid element separately: first, the equation to be solved is locally recast in integral form,

and the integral over the element is expressed with the Simpson rule; then, the extra unknown allocated at the midpoint of the element is expressed through the Numerov interpolation in terms of the two nodal unknowns belonging to the same element. The error term of the Simpson rule is of the same order as that of the Numerov process, so the accuracy of the latter is preserved. The effectiveness of the scheme has been tested on a model problem, in which both amplitude and oscillation frequency of the solution increase when one of the ends of the integration domain is approached. The method compares favorably with other methods that extend NP over a non-uniform grid, and with ML.

In the last part of the paper it has been shown how a suitable variable transformation gives the mathematical model of semiconductor devices a form amenable to the application of the Numerov process; this variable transformation makes the Numerov process applicable also to the multi-dimensional case, at least when a tensor-product, uniform grid is considered [14], [15]. On the other hand, the transformed version of the model can also be used on more general grids, whose elements are simplexes; since the extension of the Numerov process to such grids is still wanting, the solution is tackled by standard schemes like, e.g., the Box-Integration Method. The conclusions are enriched by the observation that the variable transformation illustrated in the paper is beneficial also when standard solution schemes are used; in fact, it eliminates a long-unsolved difficulty connected to the calculation of the current-density vector within each grid element.

References

1. Buturla, E.M., Cottrell, P.E., Grossman, B.M., Salsburg, K.A.: Finite-Element Analysis of Semiconductor Devices: The FIELDAY Program. IBM J. of Res. and Dev. **25**(4), 218–231 (1981). DOI 10.1147/rd.254.0218
2. Chow, P.C.: Computer Solutions to the Schrödinger Equation. American J. of Physics **40**, 730–734 (1972)
3. Cottrell, P.E., Buturla, E.M.: Two-Dimensional Static and Transient Simulation of Mobile Carrier Transport in a Semiconductor. In: B.T. Browne, J.J.H. Miller (eds.) Proc. of the NASECODE I Conference, pp. 31–64. Boole Press, Dublin (1979)
4. Forghieri, A., Guerrieri, R., Ciampolini, P., Gnudi, A., Rudan, M., Baccarani, G.: A new discretization strategy of the semiconductor equations comprising momentum and energy balance. IEEE Trans. on CAD of ICAS **CAD-7**(2), 231–242 (1988)
5. Gnudi, A., Odeh, F., Rudan, M.: Investigation of non-local transport phenomena in small semiconductor devices. European Trans. on Telecommunications and Related Technologies **1**(3), 307–312 (77–82) (1990)
6. Graen, T., Grubmüller, H.: NuSol–Numerical solver for the 3D stationary nuclear Schrödinger equation. Computer Physics Communications **198**, 169–178 (2016)
7. Kierzenka, J., Shampine, L.F.: A BVP Solver based on residual control and the MATLAB PSE. ACM Trans. Math. Softw. **27**(3), 299–316 (2001)
8. Numerov, B.: A new method for determining the orbits and calculating the ephemerides accounting for the perturbations. Publ. Obs. Central Astrophys. **2**, 188–288 (1923 (in Russian))
9. Press, W.H., Flannery, B.R., Teukolsky, S.A., Wetterling, W.T.: Numerical Recipes — The Art of Scientific Computing. Cambridge University Press, New York (1988)
10. Rudan, M.: Physics of Semiconductor Devices. Springer (2018)

11. Rudan, M., Odeh, F.: Multi-Dimensional Discretization Scheme for the Hydrodynamic Model of Semiconductor Devices. COMPEL **5**(3), 149–183 (1986)
12. Rudan, M., Odeh, F., White, J.: Numerical Solution of the Hydrodynamic Model for a One-Dimensional Semiconductor Device. COMPEL **6**(3), 151–170 (1987)
13. Scharfetter, D.L., Gummel, H.: Large-signal analysis of a silicon Read diode oscillator. IEEE Trans. Electron Dev. **ED-16(1)**, 64–77 (1969)
14. Speciale, N., Brunetti, R., Rudan, M.: Extending the Numerov Process to the Semiconductor Transport Equations. In: D. Esseni, P. Palestri, D. Rideau (eds.) 2019 International Conference on Simulation of Semiconductor Processes and Devices (SISPAD 2019), pp. 37–40. IEEE, Udine, Italy (2019)
15. Speciale, N., Brunetti, R., Rudan, M.: Solution of the Semiconductor-Device Equations by the Numerov Process. Advances in Science, Technology and Engineering Systems Journal **5**(6), 1414–1421 (2020)
16. Vigo-Aguiar, J., Ramos, H.: A variable-step Numerov method for the numerical solution of the Schrödinger equation. Journal of Mathematical Chemistry **37**(3), 255–262 (2005)

Appendix — The Numerov Process

An interpolation scheme more refined than the parabolic one is the so-called *Numerov Process* [8] (cited in [2]), which applies to second-order equations of the form

$$-u'' = F(u, x)\,. \tag{40}$$

The essence of the method is that the derivatives of the odd order are canceled, while those of even order are recursively reconstructed in terms of u by means of (40). Considering a uniform grid of size h, the nodal value at u_{i+1} is obtained by means of a Taylor expansion starting from u_i; truncating the expansion to the 5th order yields

$$u_{i+1} \simeq u_i + h\,u_i' + \frac{h^2}{2}\,u_i'' + \frac{h^3}{6}\,u_i^{(3)} + \frac{h^4}{24}\,u_i^{(4)} + \frac{h^5}{120}\,u_i^{(5)} \tag{41}$$

and, similarly,

$$u_{i-1} \simeq u_i - h\,u_i' + \frac{h^2}{2}\,u_i'' - \frac{h^3}{6}\,u_i^{(3)} + \frac{h^4}{24}\,u_i^{(4)} - \frac{h^5}{120}\,u_i^{(5)}\,. \tag{42}$$

Adding (42) to (41),

$$u_{i-1} - 2\,u_i + u_{i+1} = h^2\,u_i'' + \frac{h^4}{12}\,u_i^{(4)}\,. \tag{43}$$

Now, the same form of the interpolation is obtained if the series expansion is applied to u'' instead of u; one finds in this case

$$u_{i-1}'' - 2\,u_i'' + u_{i+1}'' = h^2\,u_i^{(4)} + \frac{h^4}{12}\,u_i^{(6)}\,. \tag{44}$$

Neglecting the 6th-order term in (44) and eliminating $u_i^{(4)}$ between (43) and (44) yields

$$u_{i-1} - 2\,u_i + u_{i+1} = \frac{h^2}{12}\,\left(u_{i-1}'' + 10\,u_i'' + u_{i+1}''\right)\,. \tag{45}$$

Finally, letting $F_i = F(u_i, x_i)$ transforms (45) into

$$-u_{i-1} + 2\,u_i - u_{i+1} = \frac{h^2}{12}\,\left(F_{i-1} + 10\,F_i + F_{i+1}\right)\,, \qquad i = 1, 2, \ldots\,. \tag{46}$$

This interpolation is obtained by keeping terms up to the 5th order; as a consequence, its precision is better than that of the parabolic interpolation. The additional computational cost is due to the right hand side of (46), whose calculation requires one more multiplication and two more additions with respect to that of the right hand side of standard finite-difference scheme; the cost of inverting the matrix of the algebraic system (46) is, instead, the same.

As anticipated, the method eliminates (without approximations) the odd-order derivatives and exploits the form of the equation to eliminate the even-order ones. This does not mean that the calculation of the odd-order derivatives is prevented; in fact, subtracting (42) from (41) one obtains

$$u_{i+1} - u_{i-1} = 2\,h\,u'_i + \frac{h^3}{3}\,u^{(3)}_i + \frac{h^5}{60}\,u^{(5)}_i\,. \tag{47}$$

Neglecting the 5th-order term in (47) and repeating the calculation for u'',

$$u''_{i+1} - u''_{i-1} = 2\,h\,u^{(3)}_i + \frac{h^3}{3}\,u^{(5)}_i\,. \tag{48}$$

Neglecting again the 5th-order term and eliminating $u^{(3)}_i$ between (47) and (48),

$$u_{i+1} - u_{i-1} = 2\,h\,u'_i + \frac{h^2}{6}\,\left(u''_{i+1} - u''_{i-1}\right)\,, \tag{49}$$

which is rearranged as

$$u'_i = \frac{u_{i+1} - u_{i-1}}{2\,h} + \frac{h}{12}\,\left(F_{i+1} - F_{i-1}\right)\,. \tag{50}$$

The calculation of the derivative keeps the terms up to the 4th order. It is also important to note that (50) provides the derivative at the ith node, not within one or the other neighboring elements like in the parabolic approximation.

Still considering (40), it is convenient to consider separately the case where the dependence of F on u is linear, namely,

$$F = c\,u + s\,, \tag{51}$$

where c, s are two given functions of x, from the case where the dependence is non linear. In the linear case (46) and (50) become, respectively,

$$-\left(1 + \frac{h^2}{12}\,c_{i-1}\right)\,u_{i-1} + \left(2 - 10\,\frac{h^2}{12}\,c_i\right)\,u_i - \left(1 + \frac{h^2}{12}\,c_{i+1}\right)\,u_{i+1} =$$

$$= \frac{h^2}{12}\,\left(s_{i-1} + 10\,s_i + s_{i+1}\right)\,, \tag{52}$$

$$u'_i = \left(\frac{1}{2\,h} + \frac{h}{12}\,c_{i+1}\right)\,u_{i+1} - \left(\frac{1}{2\,h} + \frac{h}{12}\,c_{i-1}\right)\,u_{i-1} + \frac{h}{12}\,\left(s_{i+1} - s_{i-1}\right)\,. \quad (53)$$

In the non-linear case, which is typical of, e.g., the mathematical model of semiconductor devices, one must preliminarily linearize (40) starting from a tentative solution $\bar{u}$; specifically, one lets $u = \bar{u} + \delta u$, this transforming (40) into

$$-\bar{u}'' - \delta u'' = F(\bar{u} + \delta u, x) \simeq F(\bar{u}, x) + \left(\frac{\partial F}{\partial u}\right)_{\bar{u}}\,\delta u\,, \quad (54)$$

which must then be solved by iterations. When dealing with (54) one may still use (52) and (53) provided the following replacements are used:

$$u \leftarrow \delta u\,, \qquad c \leftarrow \left(\frac{\partial F}{\partial u}\right)_{\bar{u}}\,, \qquad s \leftarrow \bar{u}'' + F(\bar{u}, x)\,. \quad (55)$$

At convergence, $\delta u = 0$ and $-\bar{u}'' = F(\bar{u}, x)$.

Declarations

Funding: Not applicable.

Conflicts of interest/Competing interests: Not applicable.

Availability of data and material (data transparency): Data and material are available.

Code availability: Code is available.

Authors' contributions: Equal contributions.

Figures

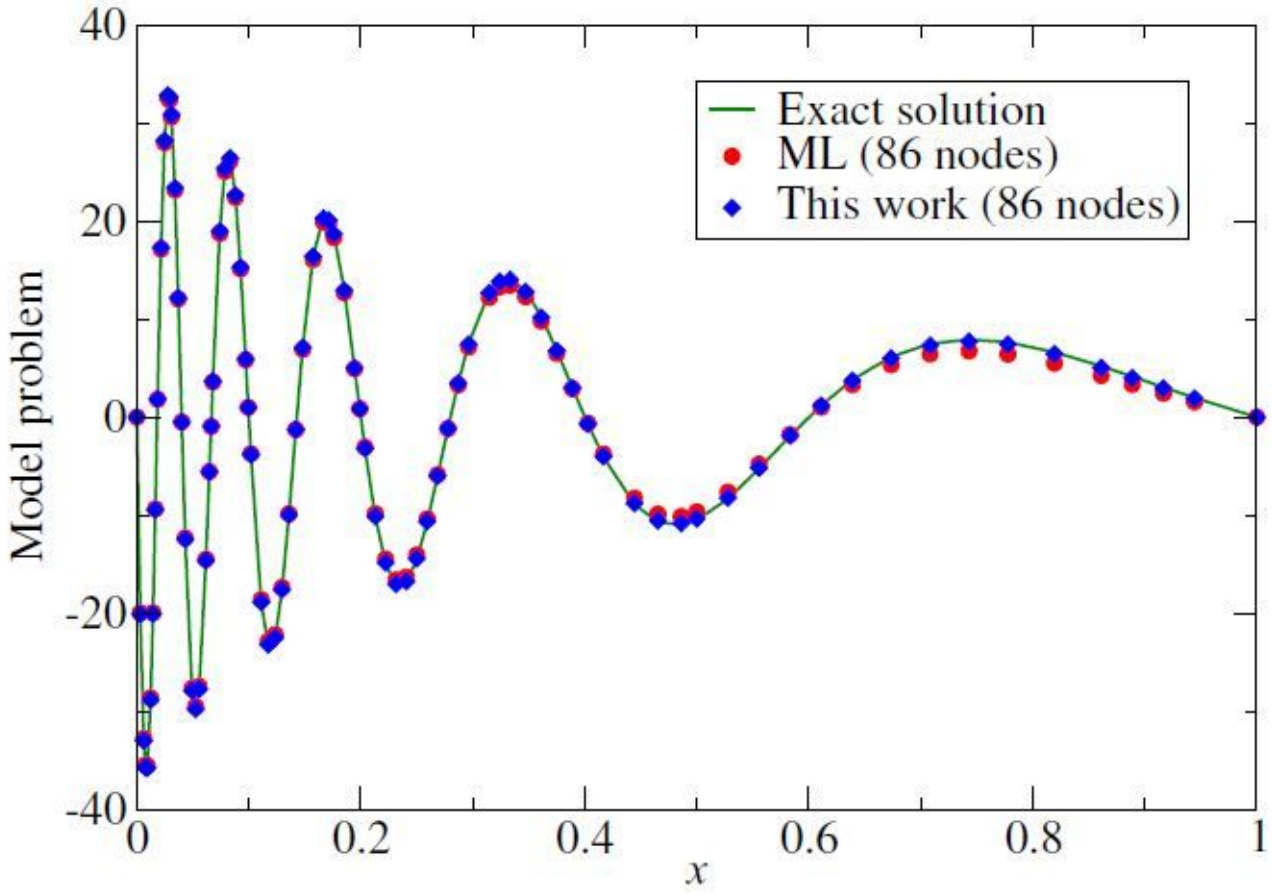

Figure 1

Comparison between the solution of the model problem obtained over an 86-node grid using ML (red circles) and the method of this work (blue diamonds). The green line shows the exact solution of the same problem (the values of the parameters in (20) are k = 2, p = 5).

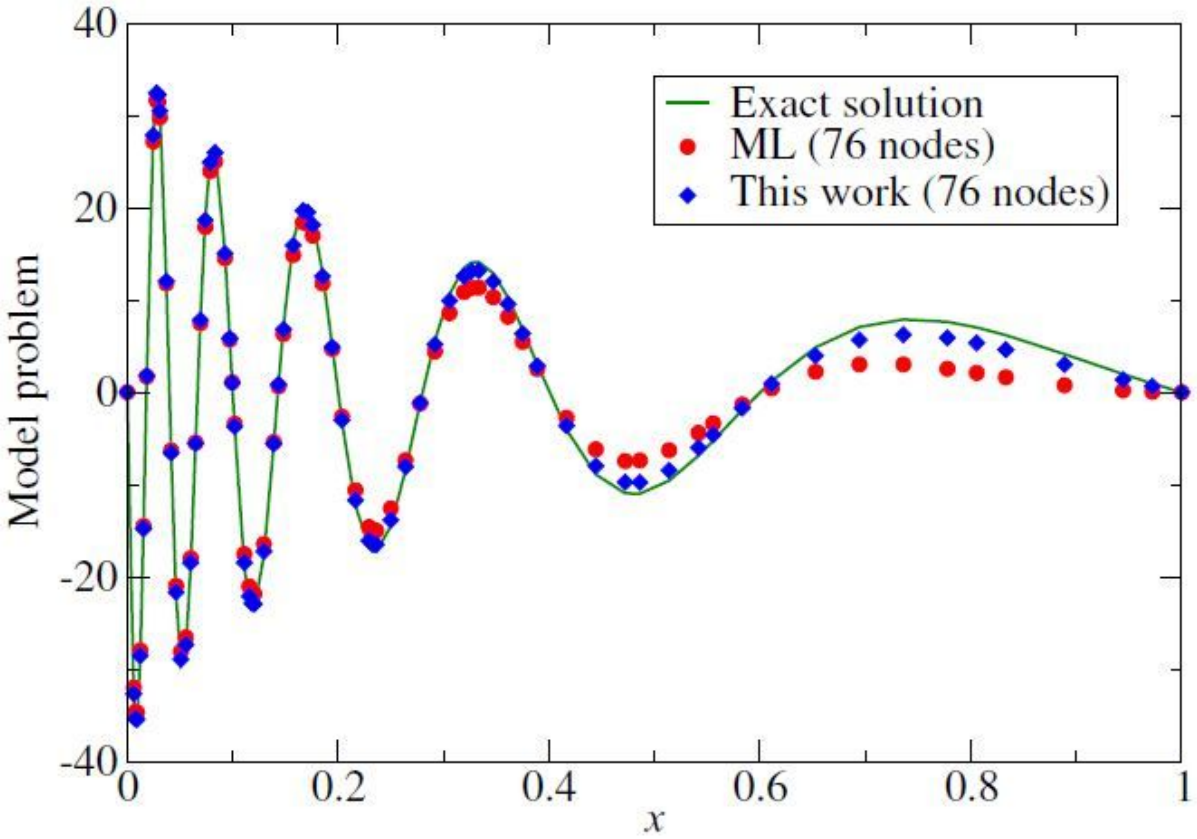

Figure 2

Comparison between the solution of the model problem obtained over a 76-node grid using ML (red circles) and the method of this work (blue diamonds). The green line shows the exact solution of the same problem (the values of the parameters in (20) are k = 2, p = 5).

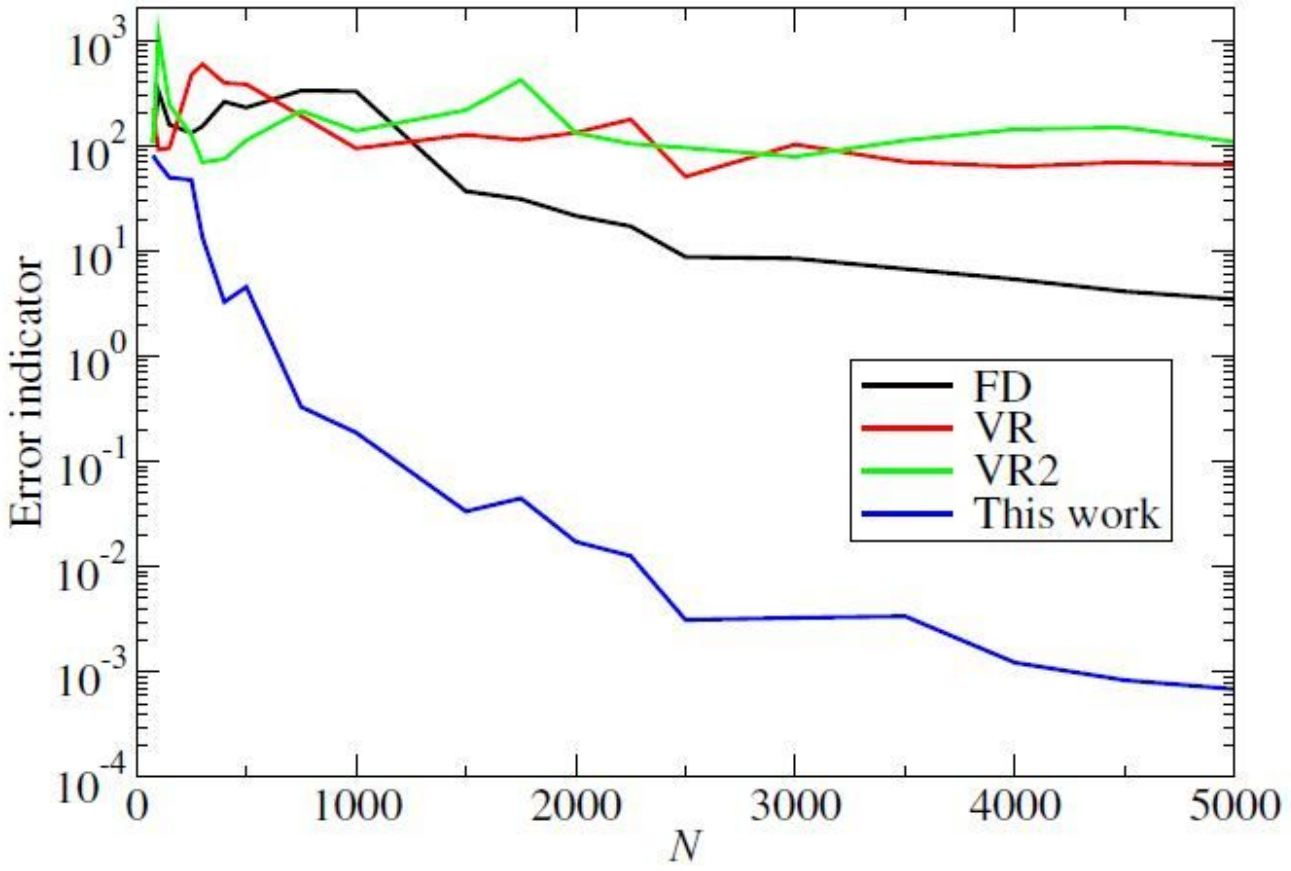

Figure 3

Error indicators (23) obtained by solving the model problem (20) over randomlygenerated grids using the FD (black line), the VR (red line), the VR2 (green line), and the non-uniform NP method (blue line). The horizontal axis shows the number of grid nodes.

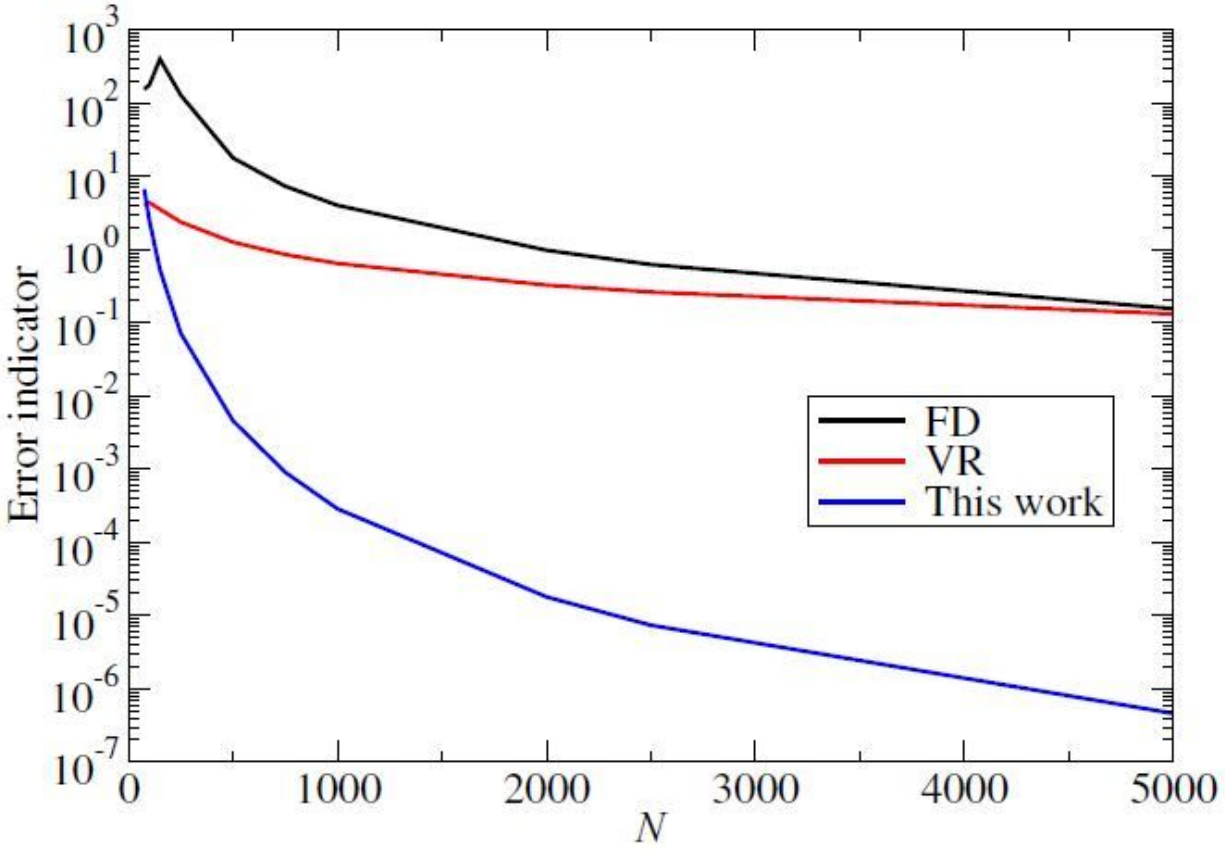

Figure 4

Error indicators (23) obtained by solving the model problem (20) over initiallyuniform grids shifted by applying the (24) scheme, using the FD (black line), the VR (red line), and the non-uniform NP method (blue line). The horizontal axis shows the number of grid nodes.

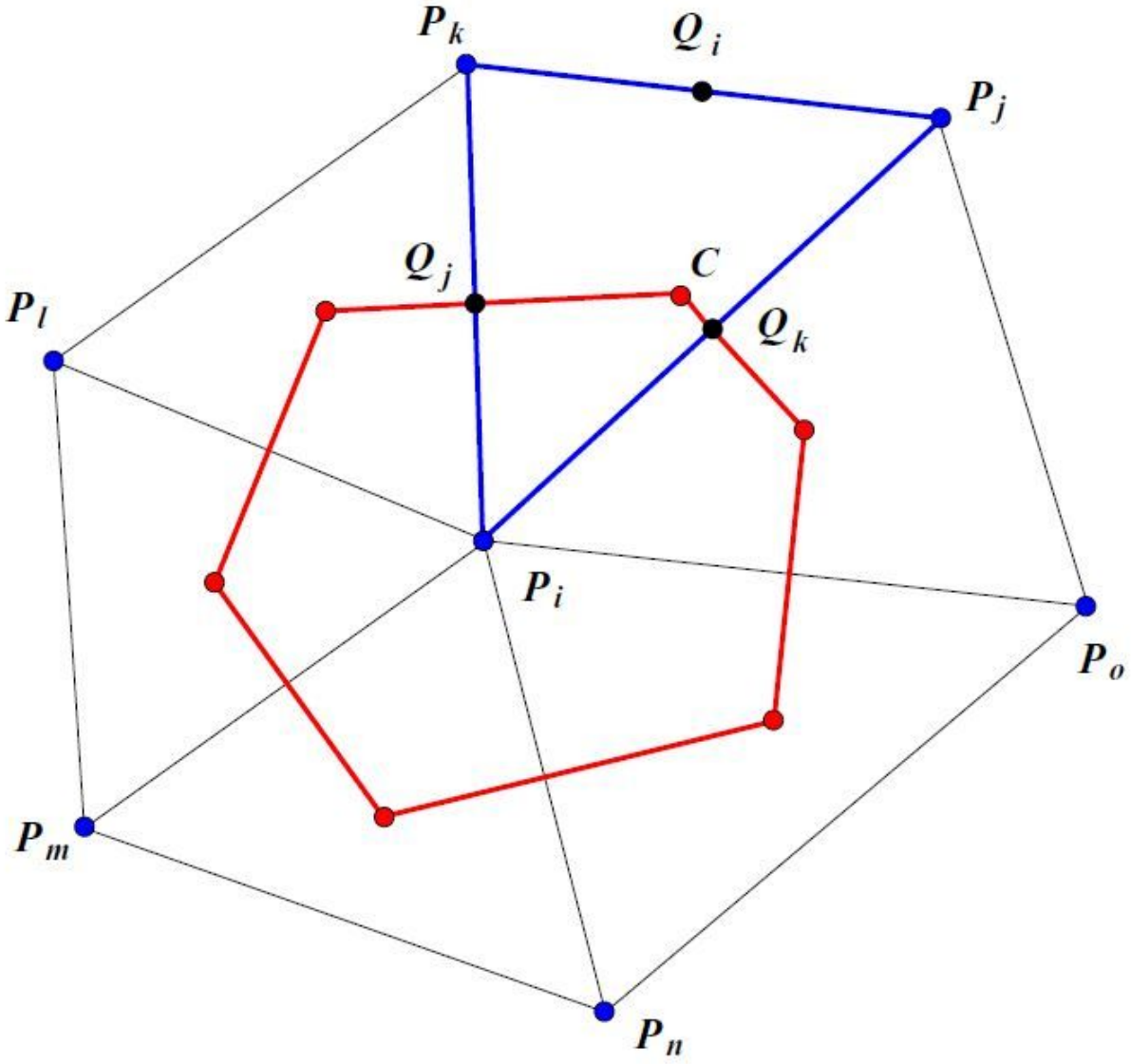

Figure 5

Example of triangle-based grid used in the simulation of semiconductor devices in two dimensions.